20 September 1999

Monitoring of the Assembly of the BOS 98 Prototype MDT Chamber

H. Kroha, A. Manz, A. Ostapchuk and S. Schael

Max-Planck-Institut für Physik, Munich

Abstract

A detailed description of the monitoring procedures and results during the construction of the BOS 98 prototype MDT chamber is given. The analysis of the optical monitoring data taken during the construction of the BOS 98 prototype chamber shows the importance of this information for the control of the assembly process. The data have been used to optimize the assembly procedure. The influence of the thermal environment in the assembly room on the chamber and on the optical monitors (laser beams) has been studied and understood in detail. The results of the analysis give confidence in the capability of the assembly method to achieve the required mechanical accuracy of the chambers in series production.

Contents

1 Introduction

The purpose of this note is to provide the details of the monitoring procedures during the construction of the BOS 98 prototype MDT chamber as a supplement to note [1] where the assembly method and measurements of the prototype chamber are described.

The description of the monitoring procedures starts after the installation and measurement of the tube jigs and the sphere support towers on the granite table and of the optical monitors on the spacer structure (see [1]). The environmental conditions in the climatized assembly room, the preparations of the sphere support towers and of the spacer are explained as well as the zero-readings of the optical monitoring devices and how they were used during chamber assembly.

The principle layout of the assembly table is shown in Figure 1 with the naming scheme for the spacer parts, cross plates CP on the high voltage (HV) and readout (RO) side and in the middle (MI) of the chamber, long beams LB-L and LB-R and spheres supported on the sphere towers T1–T6 on the table, and the different optical monitors. The following optical monitoring systems have been used extensively during assembly of the prototype:

1. The four RASNIK in-plane alignment systems IP1–IP4.
2. Three RASNIK cross plate sag monitors S-HV, S-MI and S-RO mounted on the three cross plates with the lens in the center and mask and CCDs at the ends at a distance of 1 m from the lens.
3. Two multi-point sphere monitors MP-L and MP-R with two laser beams directed parallel to the long beams on either side of the chamber and passing through several transparent MPA-ALMY sensors, reference sensors MP-LR1,2 and MP-RR1,2 on the assembly table at start and end of the laser beams and sensors MP-L1–MP-L3 and MP-R1–MP-R3 mounted on all six sphere holders at the ends of the cross plates (see [2]).

The first test of the assembly procedure was the reproducibility of the optical monitor readings when the spacer was repeatedly released on the sphere towers. The test lead to the definition of a minimum of mechanical constraints of the sphere towers on the spacer needed for the correct relative orientation of the two multilayers.

After good reproducibility of the spacer positioning on the sphere towers was achieved, the optical monitor readings in the initial and the inverted orientation of the spacer on the towers were compared. The spacer is inverted by rotations of 180° around the x- and the y-axis (see Figure 6). The comparison provides an information about the relative height of the six sphere supports.

Finally, the monitor readings in the two orientations of the spacer on the granite table were compared with the readings in four orientations of the spacer supported on the crane used for assembly: the two vertical and the two horizontal orientations (see Figure 7). This study leads to a procedure to adjust the long-beams to the center of the middle cross plate in order to avoid internal stresses and to minimize up-down asymmetries in the gravitational sag of the cross plates and left-right asymmetries in the sag of the long beams.

After completion of the above steps, the zero-readings of the RASNIK monitors on the spacer could be taken to be available as references during the assembly of the chamber. During chamber construction, the stability of the monitor readings was studied which is essential for

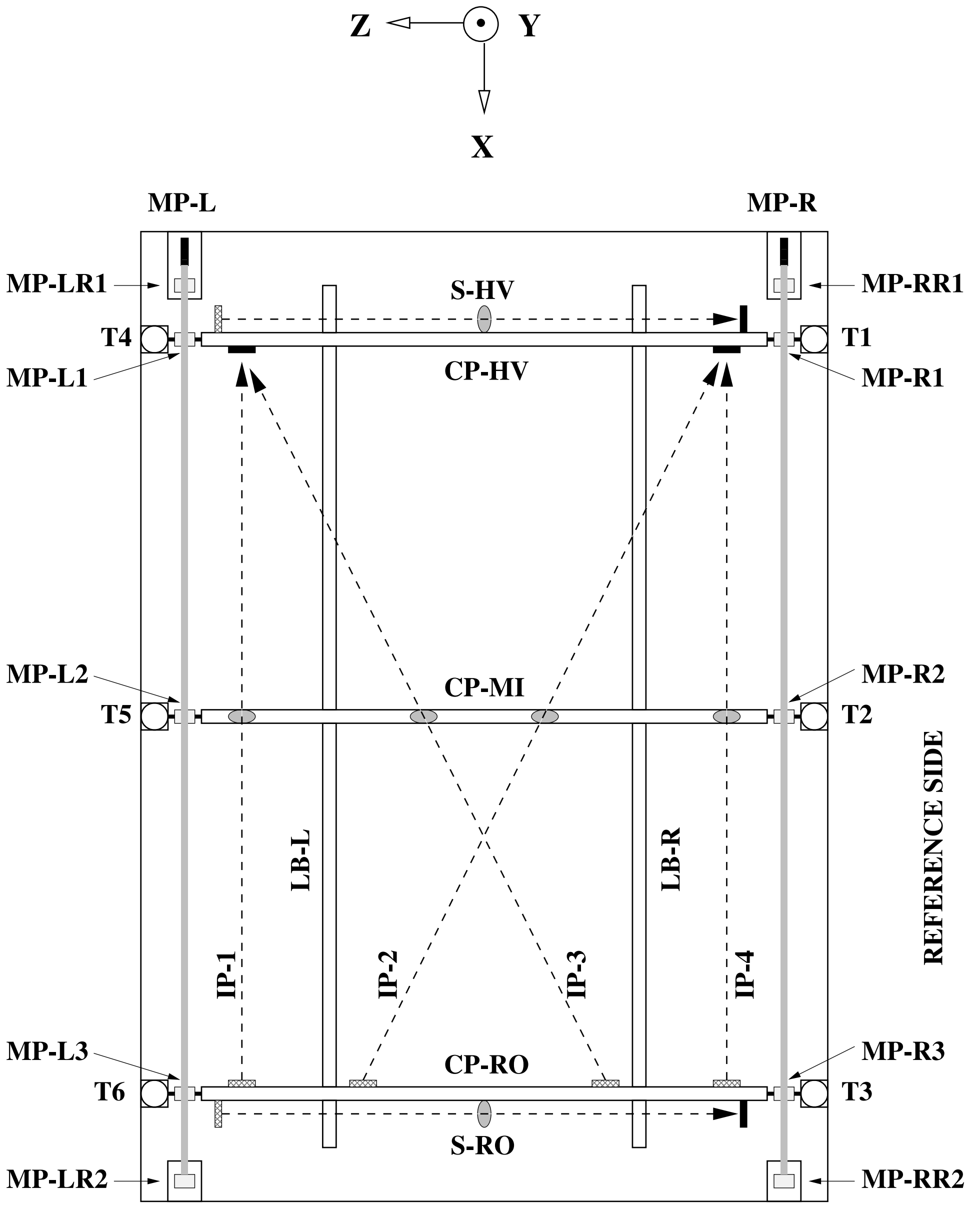

Fig. 1: Layout of the chamber assembly table and chamber coordinate system with the spacer support structure on the table in the initial (INI) orientation. The naming of the spacer components and optical monitoring devices is explained in the text.

the performance of the assembly procedure and for the prediction of the mechanical properties of the chamber.

2 Preparations Before Assembly

2.1 Temperature Control in the Assembly Room

The BOS prototype chamber was assembled in a climatized clean room with the following specifications in accordance with [3]: humidity $(45 \pm 5)\%$ and air temperature above the assembly table (20 ± 0.5)°C. Temperature and humidity were monitored during the chamber construction with an analog plotter device. The continuous monitoring revealed a cycle of the air conditioning system with a period of 30 minutes and amplitudes of temperature and humidity variations within the tolerances.

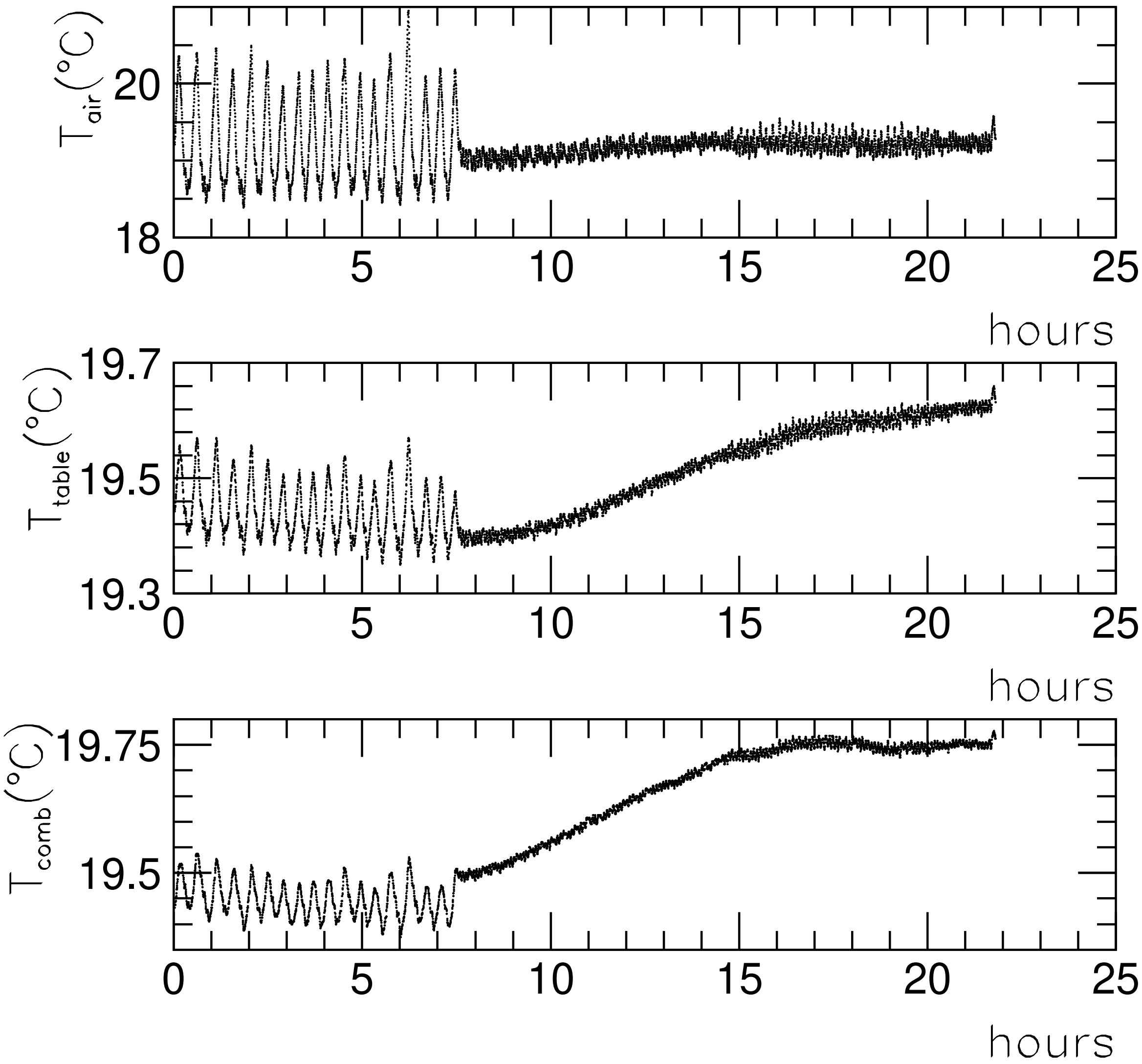

Fig. 2: Temperature measured in the climatized assembly room over a period of 24 hours in the air and at the top (combs) and bottom of the granite table (see text)

After the prototype construction, the clean room was equipped with a set of 12 high-precision temperature sensors, 4 sensors at the corners of the bottom side of the granite table, 4 sensors attached to the ends of the two end combs on top of the assembly table and 4 sensors distributed in the room to measure the air temperature. One of them was delivered with absolute calibration by the manufacturor. The others were calibrated with respect to the reference sensor. Both the measurement resolution and the calibration accuracy are better than ±0.05°C. The sensors can be read out continuously with a LabVIEW program on a PC.

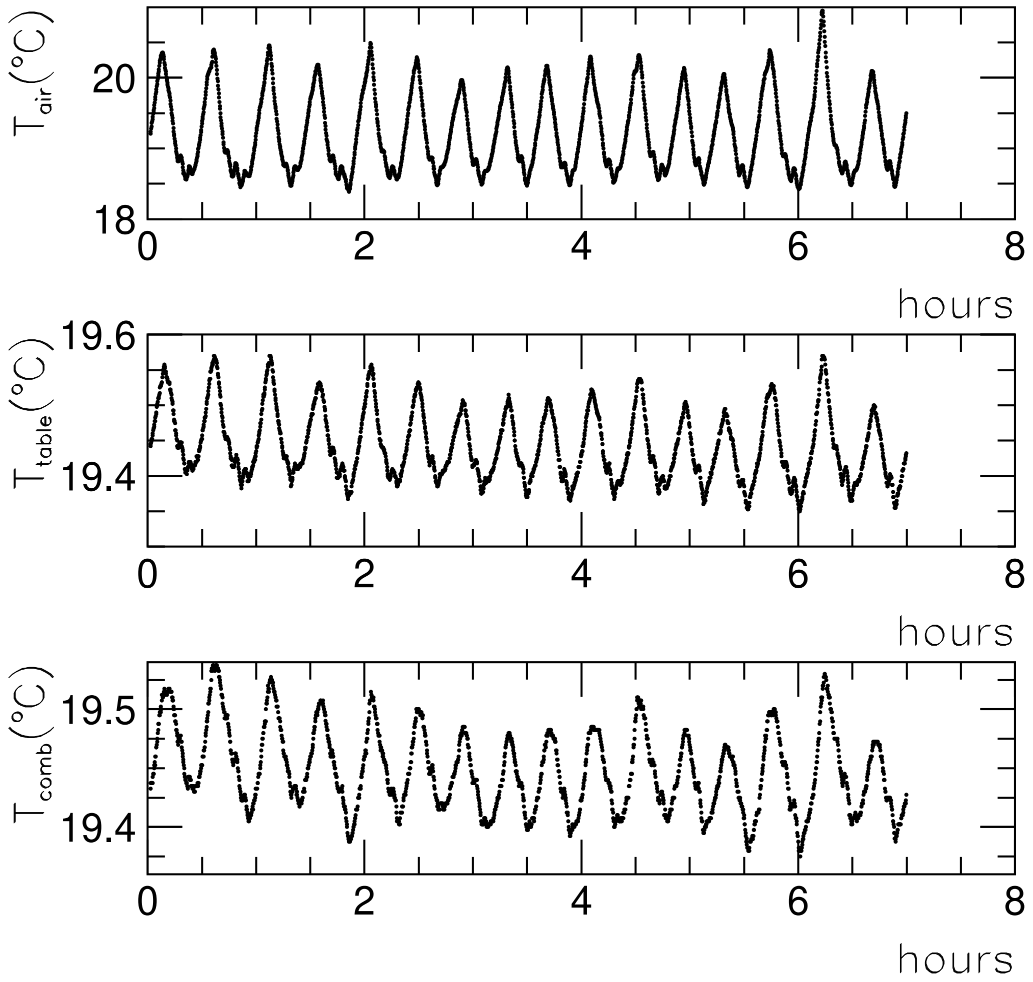

Fig. 3: As Figure 2 with the night period enlarged

The purpose of the measurements was to determine with high accuracy

1. the stability of the air temperature in the clean room,
2. the uniformity of the air temperature and
3. the stability and uniformity of the temperature of granite table and combs.

The first observation was that the air conditioning system operates in two regimes with different characteristics: *cooling* when the incoming air from outside the clean room is warmer than the air inside, and *heating* when the input air temperature is lower than the clean room temperature. In the first case, the air temperature in the clean room oscillates with an amplitude of ± 0.1°C and a period of about 5 minutes. In the second regime, the amplitude of the air temperature oscillations in the clean room is ± 1°C with a period of approximately 30 minutes. The measured temperature variations over a 24 hour period are shown in Figures 2, 3 and 4. The two regimes can be clearly distinguished: the cooling regime during the day and heating during the night.

The BOS 98 prototype was assembled in February 1998 when the outside air temperature was always below the specified clean room temperature. Therefore the air conditioning system

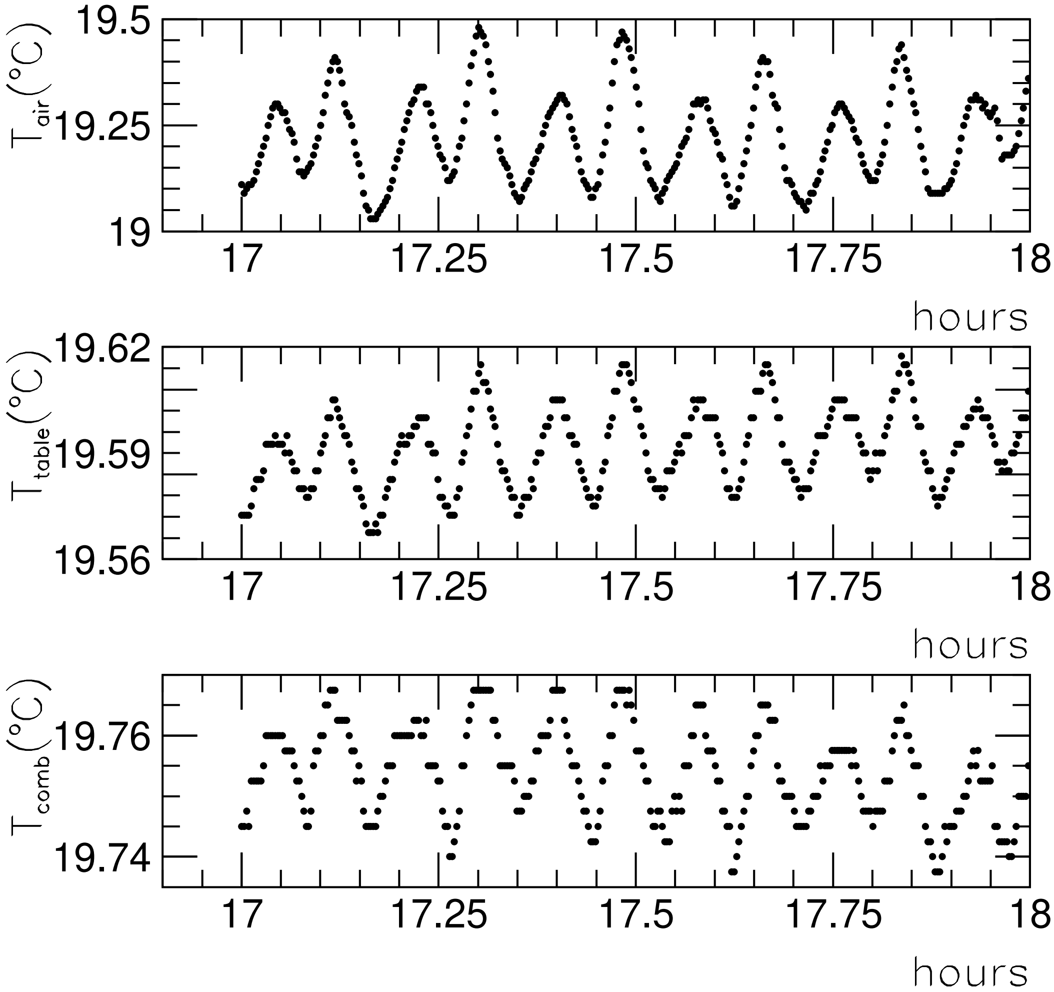

Fig. 4: As Figure 2 with the day period enlarged

worked in the heating regime with the larger air temperature variations of ±1°C at a period of 30 minutes which also was observed during the chamber construction.

To study temperature gradients in the air, four sensors were placed in different locations in the clean room: one on the wall in a corner of the room close to the floor, one at the same height in an opposite corner, one at 3 meters height above the first sensor and the fourth sensor at a distance of 5 cm above the granite table. No temperature differences larger than ±0.1°C have been detected between the four sensors in both air conditioning regimes.

The four temperature measurements at the bottom of the granite table agree with each other with an accuracy of ±0.1°C. The same is true for the four measurements on top of the granite table at the combs. The averages of the temperature measurements in the four corners at the top (on the combs) and at the bottom of the granite table are shown in Figures 2, 3 and 4. The temperature variations of granite table and combs are much smaller than the periodic temperature variations of the air in both air conditioning regimes.

There is, however, a small temperature gradient between the granite table surface and the air (see Figure 5). The average temperature difference of the bottom of the granite table with respect to the air is +0.22°C during the night and +0.34°C during the day. The combs on top of the table show an average temperature difference relative to the air of +0.22°C during the

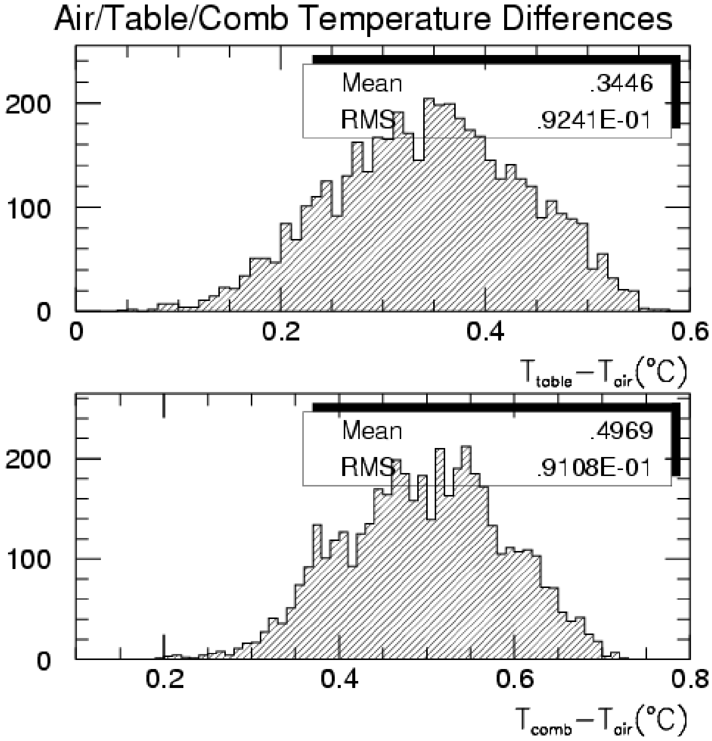

Fig. 5: Temperature differences with respect to the air of the top and of the bottom of the granite table in the clean room during the day

night and of +0.50°C during the day. Therefore there is an average temperature difference of maximum +0.16°C between top (combs) and bottom of the granite table only during the day which is within the range recommended by manufacturers for a long lifetime of the flatness of the granite table (see [5]).

The temperature difference between granite table and air can be explained by the illumination of the assembly room heating the granite table. The electric lights were switched on continuously during the measurements shown. After switching off the lights in the clean room, the temperature of the granite table approaches the average air temperature during the night. During the day there is an additional source, most likely the day-light, heating mostly the top surface of the granite table.

The temperatures of the end combs define the z-pitch of the tube layer placed on them. The z-pitch of the tube layers already glued to the spacer is also sensitive to the air temperature. The maximum difference between comb pitch and z-pitch of the tube layers already glued to the spacer which can be caused by the observed temperature difference of 0.4°C between combs and air is

$$\Delta_z = 0.4°\mathrm{C} \cdot 27\ \frac{\mu\mathrm{m}}{\mathrm{m}\ °\mathrm{C}} \cdot \frac{2.160\ \mathrm{m}}{72} \simeq 0.3\ \mu\mathrm{m}.$$

If this difference in pitch between successive tube layers were completely frozen in the chamber it would be at the limit of what can be tolerated for the precision of the chamber.

During the prototype assembly, the lights in the clean room were switched off during the night when the glue between successive tube layers was curing. The z-pitch of the 6 tube layers of the prototype chamber is very uniform with a maximum variation of 0.4 μm on the high-voltage and the readout side as verified by the X-ray tomograph measurements (see [4]).

2.2 Constraints of the Sphere Towers

Originally [3] the sphere support towers provided the following mechanical constraints on the spacer orientation on the assembly table: the sphere support of tower T1 was fixed both in x- and in z-direction, the sphere supports of towers T2 and T3 were only free in x-direction and fixed in z and the spheres on towers T4, T5 and T6 were free both in x- and in z-direction.

The results of the reproducibility test with this setup are shown in Table 1. The spacer was set on the sphere towers, lifted with the crane and released again several times. Every time the spacer was released on the sphere towers the crane was disconnected and the crane supports on the spacer were dismounted.

Table 1: Reproducibility of the (longitudinal) in-plane monitor readings before releasing the z-constraint of sphere tower T2

Attempt	$y_{\mathrm{IP}-1}$ [μm]	$y_{\mathrm{IP}-4}$ [μm]	$z_{\mathrm{IP}-1,4}$ [μm]
1	4	2	1-2
2	20	25	20-30
3	2	6	5-7

The in-plane monitor readings varied by about $20-30$ μm in these tests and were also unstable. It was found that the sphere supports in their original configuration over-constrained the spacer structure when it was inverted, namely the z-position of the middle cross plate. This led to irreproducible positioning of the spheres on tower T2 in z and y measured by the in-plane monitors. After releasing the z-constraint on sphere tower T2, the reproducibility of the monitor readings improved to the expected level of a few micron.

2.3 Test of Sphere Tower Planarity

The planarity of the system of six sphere towers can be verified by comparing the in-plane monitor readings in the initial and the inverted orientation of the spacer. As explained in Figure 6, half the difference in the y-readings of in-plane monitor IP-1 in the two spacer orientations determines the deviation of the heights on the sphere towers T4, T5 and T6 from a straight line. The same applies for towers T1–T3 and monitor IP-4. Equal height of the towers on the right- and the left-hand side cannot be tested with this method.

The y-readings of monitor IP-1 showed an initial deviation of -25 μm of the height of tower T5 from the line connecting towers T4 and T6 which was confirmed by direct measurement and corrected. After the correction, the test showed deviations of both tower lines, T1–T3 and T4–T6, from a straight line of not more than $\pm$ a few micron.

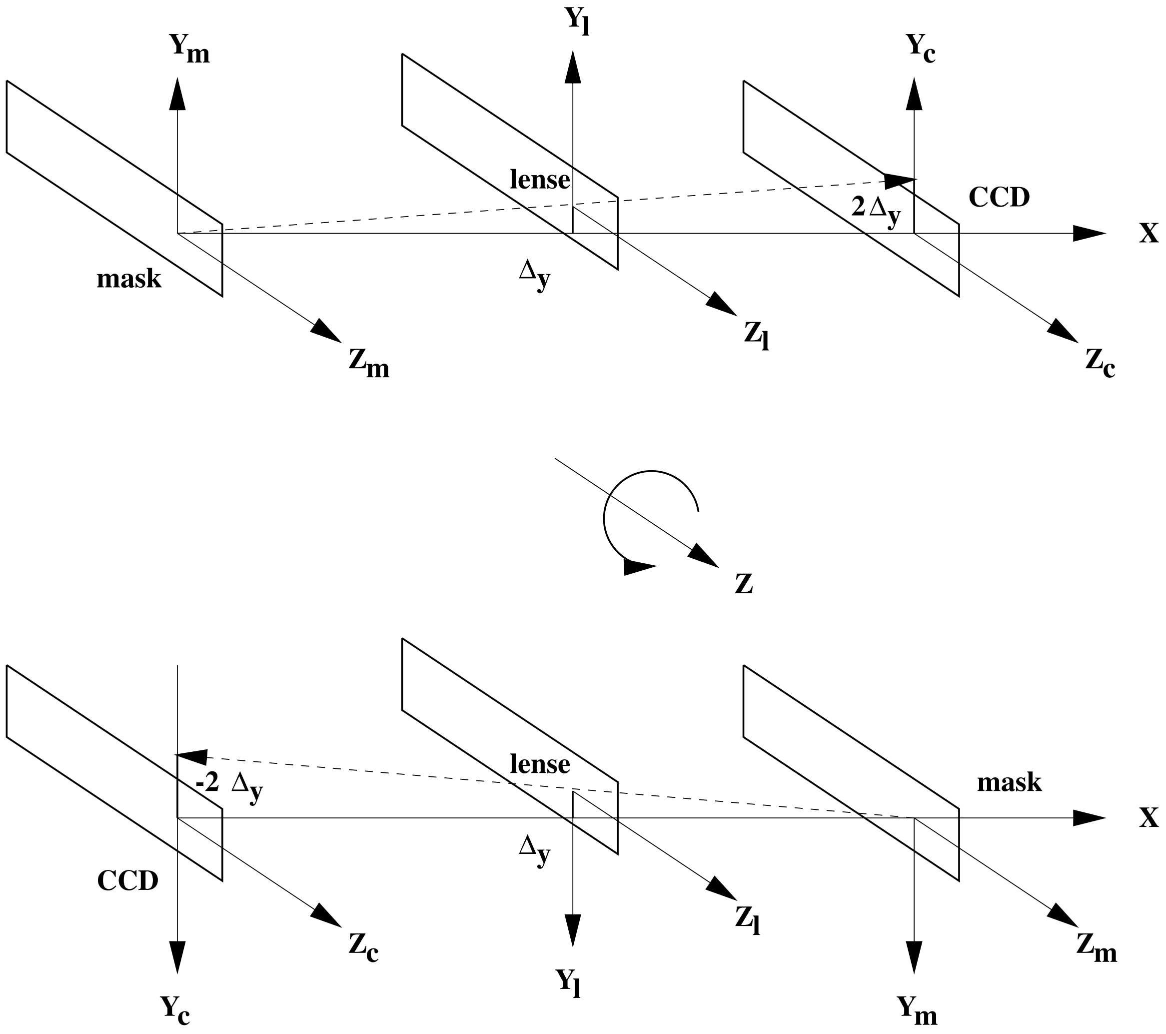

Fig. 6: Effect of unequal height of the sphere towers on the y-readings of the in-plane monitors

2.4 Preparation of the Spacer

The in-plane and cross plate RASNIK systems were continuously operational during the chamber construction including when the spacer was supported on the crane and not on the assembly table. Comparison of the readings of the RASNIK monitors in the four orientations of the spacer on the crane, two vertical (V1, V2) and two horizontal (H1, H2) orientations (see Figure 7), and in the two orientations, initial (INI) and inverted (INV), of the spacer on the sphere towers allows to detect internal stresses of the assembled spacer. Using this information, the long-beam fixations on the middle cross plate were adjusted to the center of the cross plate in order to minimize internal stresses caused by asymmetric fixation. Such built-in stresses lead to unpredictable up-down asymmetric sag of the cross plates and left-right asymmetric sag of the chamber along the long beams.

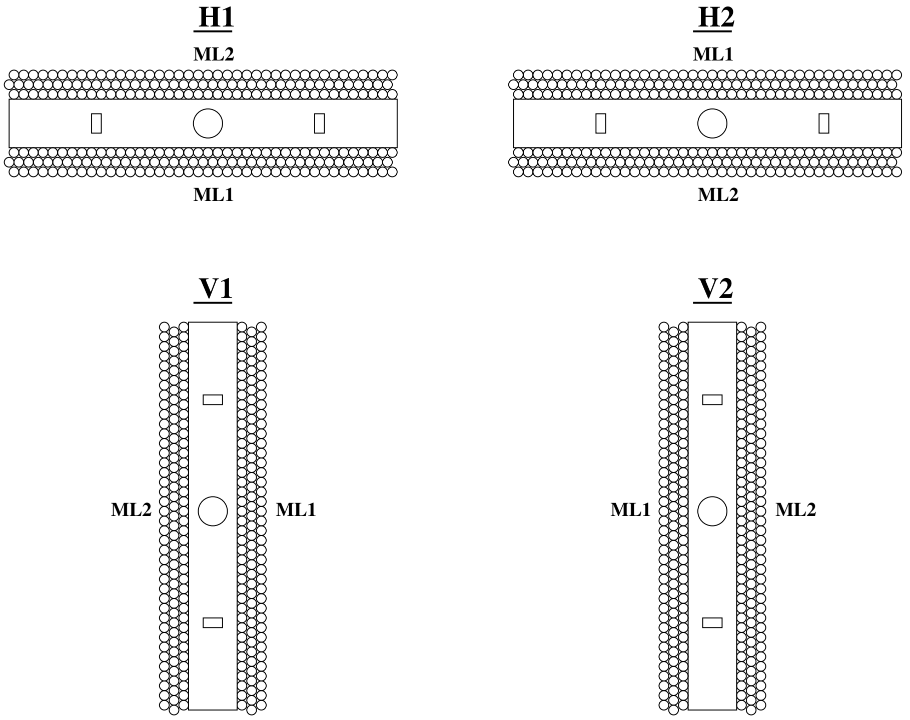

Fig. 7: The four orientations of the chamber when supported on the crane

2.4.1 Adjustment of the Long-Beam Fixations

Initially, the long-beams were fixed to the middle cross-plates in preliminary positions close to their median plane. The y-readings of the longitudinal in-plane monitors IP-1 and IP-4 in four successive states of the spacer, INI, V1, V2, INV, before further adjustments are shown in Table 2.

The readings in the states INI and INV are equal for each monitor since they are defined by the height of the sphere towers. Without internal stresses in the spacer, the monitor readings in the vertical orientations V1 and V2 on the crane are expected to be the same as for the spacer on the sphere towers since there are no forces to deform the spacer. The data in Table 2 indicate a torsional deformation of the spacer in the vertical orientations on the crane which can be explained by internal stresses in the spacer due to imperfect centering of the long beam fixations on the middle cross plate.

The difference between the in-plane monitor readings in the two vertical orientations can be explained by measurement errors in the y- and z-coordinates due to the unknown relative angular orientations of masks and CCDs of the RASNIK monitors. The relative vertical displacement of the middle cross plate between the states V1 and V2 (sag in z-direction in the chamber coordinate frame) is as large as $\sim 5\ mm$. If masks and CCDs are not perfectly aligned which was not attempted, the large displacement leads to sizable differences also in the horizontal (y-) readings of the in-plane monitors in orientations V1 and V2.

The internal stresses of the spacer have an additional consequence. In the absence of stresses, the cross-plates should show no deformations in the vertical orientations on the crane and the gravitational sags of the cross plates in the states INI and INV should be of equal size with respect to vanishing sag in the vertical states V1 and V2.

Table 2: The y-readings [mm] of the longitudinal in-plane monitors IP-1 and IP-4 and of the sag monitors S-RO, S-MI and S-HV on the three cross plates in the initial (INI) and inverted (INV) orientations of the spacer on the sphere towers and in the vertical positions V1 and V2 on the crane and the average of the latter **before** adjustment of the long beams. The gravitational sags [μm] of the cross plates in the INI and INV positions calculated from these readings are also given.

Orientation	$y_{\mathrm{IP-1}}$ [mm]	$y_{\mathrm{IP-4}}$ [mm]	$y_{\mathrm{S-RO}}$ [mm]	$y_{\mathrm{S-MI}}$ [mm]	$y_{\mathrm{S-HV}}$ [mm]	$\mathrm{Sag}_{\mathrm{CP-RO}}$ [μm]	$\mathrm{Sag}_{\mathrm{CP-MI}}$ [μm]	$\mathrm{Sag}_{\mathrm{CP-HV}}$ [μm]
INI	16.841	17.039	10.377	13.834	10.403	55	−7	56
V1	17.203	17.422	10.263	13.846	10.289			
V2	17.129	17.472	10.271	13.845	10.292			
$< V1, V2 >$	17.166	17.457	10.267	13.846	10.291			
INV	16.866	17.043	10.252	13.675	10.269	8	86	11

The gravitational sags of the cross-plates in the INI and INV states can be calculated from the corresponding y-readings of the cross plate RASNIK monitors in Table 2 and the average of the y-readings in the two vertical orientations as reference according to the following relations (the factor 1/2 arises from the conversion of RASNIK readings, i.e. displacement of the mask image on the CCD, to lens displacement):

$$\mathrm{Sag}_{CP}^{INI} = \frac{y_{\mathrm{S-CP}}^{INI} - y_{\mathrm{S-CP}}^{V}}{2},$$

$$\mathrm{Sag}_{CP}^{INV} = \frac{y_{\mathrm{S-CP}}^{V} - y_{\mathrm{S-CP}}^{INV}}{2}.$$

The sags of the three cross plates in the four states INI, V1, V2 and INV of the spacer are given in Table 2 and Figures 8 and 9. Before further adjustments of the long beams, the measured cross plate sags show a considerable asymmetry between the INI and INV orientation providing ambiguous input for the cross plate sag compensation during assembly of the tube layers.

The following model was employed for the final adjustment of the long beams to remove the internal stresses of the spacer.

The relative y-displacements of the middle cross-plate in the chamber coordinate system are considered in two states of the spacer, on the sphere-holders (INI) and in vertical orientation on the crane, as illustrated in Figure 10. The y-displacements $\Delta y_{\mathrm{IP-1,4}}$ of the lenses of the two longitudinal in-plane RASNIK monitors IP-1 and IP-4 in the vertical orientation (average for V1 and V2) relative to the reference position on the sphere towers (INI) determine the required adjustments $\Delta y_{\mathrm{LB-L}}$ and $\Delta y_{\mathrm{LB-R}}$ of the two long beams on the middle cross plate using a linear interpolation between the z-positions $z_{\mathrm{IP-1,4}}$ of the lenses:

$$\Delta y_{\mathrm{LB}-i} = -\Delta y_{\mathrm{IP-1}} - \frac{\Delta y_{\mathrm{IP-4}} - \Delta y_{\mathrm{IP-1}}}{z_{\mathrm{IP-4}} - z_{\mathrm{IP-1}}} \cdot (z_{\mathrm{LB}-i} - z_{\mathrm{IP-1}}), \quad i = L,\ R, \tag{1}$$

where $z_{\mathrm{LB}-i}$ are the z-coordinates of two long-beams on the middle cross plate.

From the data in Table 2 one derives

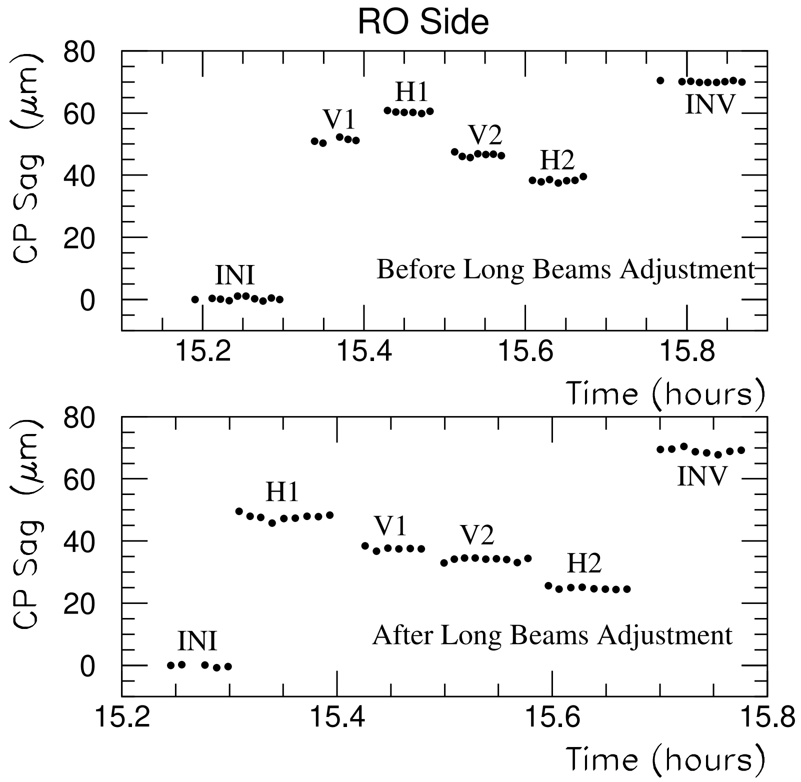

Fig. 8: y-deformations (with respect to the INI orientation) of the readout (RO)-side cross plate measured with the cross plate RASNIK monitor before and after long beam adjustment (see text) in the initial (INI) and inverted (INV) orientation of the spacer on the sphere towers and in the four orientations (V1, V2, H1, H2) of the spacer on the crane. After long beam adjustment, the cross plate sags in the INI and INV states are symmetric with respect to the bending in the vertical orientations and can be determined as the average of the INI and INV readings.

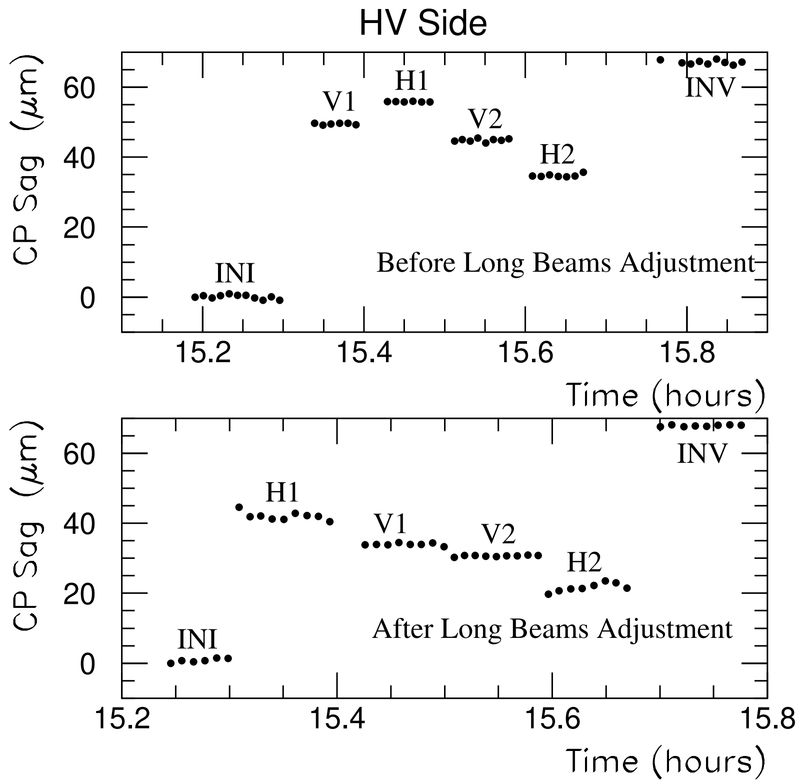

Fig. 9: Same as Figure 8 for the high voltage (HV)-side cross plate

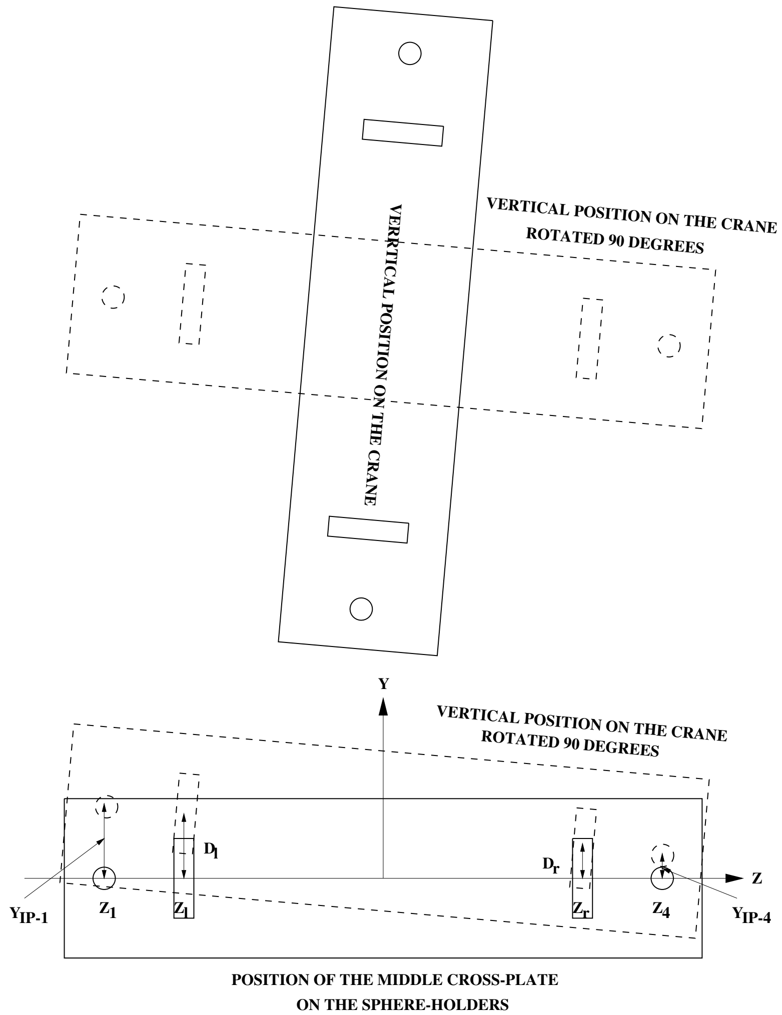

Fig. 10: Adjustment of the long beams on the middle cross plate

$$\Delta y_{\mathrm{IP-1}} = \frac{< y^{V}_{\mathrm{IP-1}} > - y^{INI}_{\mathrm{IP-1}}}{2} = 166\ \mu\mathrm{m},$$

$$\Delta y_{\mathrm{IP-4}} = \frac{< y^{V}_{\mathrm{IP-4}} > - y^{INI}_{\mathrm{IP-4}}}{2} = 206\ \mu\mathrm{m}.$$

According to equation (1) the long beam fixations on the middle cross-plate have been shifted by

$$\begin{aligned}\Delta y_{\mathrm{LB-L}} &= -y_{\mathrm{IP-1}} - \frac{\Delta y_{\mathrm{IP-4}} - \Delta y_{\mathrm{IP-1}}}{z_{\mathrm{IP-4}} - z_{\mathrm{IP-1}}} \cdot (z_{\mathrm{LB-L}} - z_{\mathrm{IP-1}}) \\ &= -166\ \mu m + \frac{206\ \mu m - 166\ \mu m}{1500\ mm} \cdot 300\ mm \simeq -150\ \mu\mathrm{m}\end{aligned}$$

and

$$\Delta y_{\mathrm{LB-R}} = -y_{\mathrm{IP-1}} - \frac{\Delta y_{\mathrm{IP-4}} - \Delta y_{\mathrm{IP-1}}}{z_{\mathrm{IP-4}} - z_{\mathrm{IP-1}}} \cdot (z_{\mathrm{LB-R}} - z_{\mathrm{IP-1}})$$
$$= -166\ \mu m - \frac{206\ \mu m - 166\ \mu m}{1500\ mm} \cdot 1200\ mm \simeq -200\ \mu\mathrm{m}$$

in the chamber coordinate frame in Figure 1 (initial orientation of the spacer).

The y-readings of the in-plane and cross-plate monitors and the corresponding cross plate sags after the adjustement are given in Table 3 and Figures 8 and 9. The cross plate sags in INI and INV orientation are now very symmetric. One concludes that internal stresses of the spacer have effectively been removed. An accuracy of 50 μm in the adjustment of the long beam fixations was sufficient to achieve this.

The residual stresses in the spacer after the adjustment still cause an asymmetry in the longitudinal gravitational sag of the chamber measured on the left- and right-hand side with monitors IP-1 and IP-4 as well as between the sag in initial and inverted orientation while the average sag of both sides is quite equal for the two chamber orientations (see Table 4). With the in-plane monitor measurements, the sag can be compensated individually for each long beam with the integrated sag compensation systems in the actual chamber orientation in the experiment. The asymmetry in the chamber sag which cannot be predicted by calculations can in principle be further reduced by adjusting the long beams with higher accuracy than 50 μm.

Table 3: The y-readings of the longitudinal in-plane monitors IP-1 and IP-4 and of the sag monitors S-RO, S-MI and S-HV on the three cross plates in the initial (INI) and inverted (INV) orientations of the spacer on the sphere towers and in the vertical positions V1 and V2 on the crane and the average of the latter **after** final adjustment of the long beams. The gravitational sags of the cross plates in the INI and INV positions calculated from these readings are also given.

Orientation	$y_{\mathrm{IP-1}}$ [mm]	$y_{\mathrm{IP-4}}$ [mm]	$y_{\mathrm{S-RO}}$ [mm]	$y_{\mathrm{S-MI}}$ [mm]	$y_{\mathrm{S-HV}}$ [mm]	$\mathrm{Sag}_{\mathrm{CP-RO}}$ [μm]	$\mathrm{Sag}_{\mathrm{CP-MI}}$ [μm]	$\mathrm{Sag}_{\mathrm{CP-HV}}$ [μm]
INI	16.759	16.985	10.316	13.933	10.353	24	37	23
V1	16.735	17.029	10.265	13.858	10.285			
V2	16.661	17.086	10.271	13.862	10.292			
$< V1, V2 >$	16.648	17.057	10.268	13.860	10.289			
INV	16.792	16.996	10.205	13.789	10.235	32	36	27

2.4.2 Thermal Properties of the Spacer

The purpose of the RASNIK cross-plate sag monitors is to measure the gravitational sag of the cross plates in y-direction during chamber assembly. But they are also able to measure cross-plate deformations in the second coordinate, in x-direction parallel to the long beams. From the continuous monitoring of the spacer stability on the sphere towers, periodic variations of bending of the cross plates in x-direction have been observed (see Figure 11) which show a clear correlation with the air temperature in the temperature controlled assembly room which varied with a period of about 20 minutes due to the control cycle of the air-conditioning system.

Table 4: Longitudinal sag (in negative y-direction) on the left- and right-hand side of the chamber supported on the crane measured with the in-plane RASNIK monitors IP-1 and IP-4 relative to their zero-readings (no sag) during assembly with increasing number of tube layers glued and after dismounting of the spheres from the completed chamber. The measurements on the pseudo-kinematic supports in the X-ray tomograph are also given.

Orientation	Initial			Inverted		
Monitor	Sag_{IP-1} [μm]	Sag_{IP-4} [μm]	Average sag [μm]	Sag_{IP-1} [μm]	Sag_{IP-4} [μm]	Average sag [μm]
Zero-reading	0	0		0	0	
Spacer	444	366	405	367	447	407
Layer 1 (ML 1)	430	356	393			
Layer 2 (ML 1)	471	394	433			
Layer 3 (ML 1)	485	416	451	424	484	454
Layer 4 (ML 2)				429	471	450
Layer 5 (ML 2)				453	502	478
Layer 6 (ML 2)	504	470	487	490	522	506
Without spheres	433	392	413	386	425	406
Tomograph support	423	381				

The measured sagittae of the two outer cross plates CP-RO and CP-HV have opposite signs and equal amplitude (about ± 5 μm while the effect for the middle cross plate is much smaller. The effect can be explained by the thermal expansion and contraction of the aluminum long-beams (by ± 10 μm corresponding to a temperature variation of the long beams of $\pm 0.1°$C) which makes the outer cross plates bend while there is little effect on the middle cross plate.

The cross plates were supported on the sphere towers at both ends during the measurements. All sphere supports except one are allowed to move in x-direction with a certain friction. Uniform expansion of the long beams and movements of the spheres in x are not measured by the assembly monitoring systems. Therefore the temperature variations and the associated length variations of the long beams could still be larger than the above estimate if the spheres at the outer cross plates moved in x-direction in addition to the observed bending of the cross plates.

In any case, the observed small deformations of the spacer in x-direction will have no impact on the chamber assembly procedure.

2.5 Zero-Readings of the RASNIK Monitors

An important step of the assembly procedure is the calibration of the RASNIK monitors. All RASNIK monitors were mounted on the spacer with a positioning accuracy of a few millimeters such that they provided sharp and analyzable images of the center area of the mask. In order to monitor deformations of the chamber during chamber assembly and afterwards, zero-readings of the RASNIK in-plane alignment and cross plate sag monitors in the non-deformed state on the assembly table have to be recorded as a reference.

The first zero-readings of the RASNIK systems at the start of the chamber construction were taken with the assembled spacer alone: as the average of the RASNIK readings in two spacer positions on the sphere towers, in the initial (INI) and in the inverted (INV) orientation. Subsequently, the stablility of the in-plane monitor readings was monitored over the whole construction. The cross plate sag monitor data were used for the compensation of the cross plate sag with the force compensation system (see [1]) before the glueing of each tube layer and to measure the cross plate sag on the supports during the X-ray tomograph measurements.

2.5.1 In-Plane Alignment System

As described above, comparison of the y-readings of the two longitudinal in-plane monitors IP-1 and IP-4 in the initial and inverted positions of the spacer on the assembly table allowed to test the planarity the sphere tower heights. After a small correction to one sphere tower, deviations from planarity and differences in the readings of the monitors for the two orientations were virtually negligible (see Table 3). The average values of the readings for both orientations were taken as zero-readings for monitors IP-1 and IP-4 during chamber construction.

The y-readings of the two diagonal in-plane monitors IP-2 and IP-3 are affected by the gravitational sag of the middle cross-plate. When the long-beam fixations on the middle cross-plate were re-adjusted to minimize internal stresses of the spacer, the gravitational sags of all cross-plates became equal in size in the initial and the inverted spacer orientation (see Table 3). This means that the average values of the y-readings of IP-2 and IP-3 in the INI and INV positions must correspond to the situation when these monitors are aligned on straight lines and therefore can be taken as the zero-readings.

The readings of the four in-plane monitors in the INI and INV positions of the spacer and their averages (the zero-readings) are given in Table 5. During chamber assembly, monitoring of the stability of the y-measurements of the in-plane monitors is essential to control the planarity of the chamber (see section 3.1, Table 7 and Figure 14).

Table 5: Zero-readings y_0 and z_0 of the in-plane RASNIK monitors at the start of chamber assembly defined as the averages of the monitor readings in the initial (INI) and the inverted (INV) spacer position on the sphere towers.

Monitor	y_{INI} [mm]	z_{INI} [mm]	y_{INV} [mm]	z_{INV} [mm]	y_0 [mm]	z_0 [mm]
IP-1	16.752	14.580	16.800	14.585	16.778	14.583
IP-2	17.344	14.343	17.476	14.346	17.407	14.345
IP-3	16.118	7.499	16.256	7.499	16.178	7.499
IP-4	16.961	10.236	17.005	10.238	16.983	10.237

After removal of the over-constraint in the sphere supports on the assembly table, differences between the z-readings of the in-plane monitors in the initial and the inverted spacer position are very small and only reflect the reproducibility of the monitor measurements themselves. After the glueing of the first tube layer to the cross plates, movements of the middle cross plate are prevented by the stiffness of the tube layers. The averages of the z-readings in INI and INV orientation were defined as the zero-readings (see Table 5) which were very stable during the whole construction with relative displacements of the middle cross plate less than 8 μm (see Table 8 and Figure 13). This shows that no significant temperature gradients occurred between the two chamber ends during the construction.

2.5.2 Cross-Plate Sag Monitors

For the cross plate sag monitors the same procedure to determine the zero-readings can be applied as for the in-plane alignment system. After the re-adjustment of the long-beams the cross-plate sags became symmetrical in the INI and INV positions such that the average values of the monitor readings for both orientations corresponded to the non-deformed state of the cross-plates. The readings of the cross-plate monitors in the two orientations and the zero-readings derived from them are given in Table 6.

Table 6: Zero-readings x_0 and y_0 of the cross plate RASNIK monitors at the start of chamber assembly defined as the averages of the monitor readings in the initial (INI) and the inverted (INV) spacer position on the sphere towers.

Monitor	x_{INI} [mm]	y_{INI} [mm]	x_{INV} [mm]	y_{INV} [mm]	x_0 [mm]	y_0 [mm]
CP-HV	14.441	10.316	14.446	10.205	14.444	10.271
CP-MI	12.846	13.933	12.843	13.789	12.845	13.865
CP-RO	12.088	10.353	12.076	10.235	12.082	10.291

3 Monitoring of the Assembly Process

3.1 In-plane Alignment System During Assembly

The role of the in-plane monitors during chamber assembly was the following:

1. Verification of the planarity of the sphere supports before glueing of each tube layer.

2. Verification of the planarity of the chamber after glueing of each tube layer.

   The readings of the in-plane monitors should be stable during the assembly process and show no significant deviations from the zero-readings.

3. Input for the reconstruction of the sag of the middle cross-plate after removal of the sag monitor on this cross plate for the assembly of the second multilayer.

4. Measurement of the longitudinal gravitational sag of the chamber for adjustment to the wire sag (separate for each long beam; see Table 4).

The deviations of the y-measurements of the in-plane monitors from their zero-readings after glueing of each tube layer are shown in Table 7 and Figure 14. Changes of the longitudinal sags of the chamber on the assembly table as measured by the in-plane monitors IP-1 and IP-4 relative to the zero-readings are below 15 μm.

During assembly of the first multilayer (tube layers 1–3), the y-readings of all monitors were very stable. Larger deviations ocurred during the assembly of the second multilayer (tube layers 4–6) which can be explained by the larger sag of the middle cross plate increasing with the number of tube layers glued (see [1] and Figure 12). The sag of the middle cross plate has no effect on the wire positioning accuracy and has not been fully compensated during the assembly of the second multilayer. The diagonal monitors IP-2 and IP-3 show about twice as large deviations from the zero-readings than the longitudinal monitors (maximum: 30 μm) since they are more affected by the sag of the middle cross plate.

The z-readings of all four in-plane monitors were very stable during the whole assembly process (see Table 8 and Figure 13).

Table 7: Stability of the y-measurements of the in-plane monitors during chamber assembly: movements of the lenses (middle cross plate) in y [μm] with respect to the zero-readings after glueing of a tube layer (0.5$\times$ the values of the y-readings shown in Figure 14).

Monitor	Layer 1	Layer 2	Layer 3	Layer 4	Layer 5	Layer 6
IP-1	-3	3	-1	8	2	9
IP-2	-6	-2	-15	15	24	13
IP-3	-2	6	0	18	22	30
IP-4	-1	1	-9	5	16	13

Table 8: Stability of the z-measurements of the in-plane monitors during chamber assembly: movements of the lenses (middle cross plate) in z [μm] with respect to the zero-readings after glueing of a tube layer (0.5$\times$ the values of the z-readings shown in Figure 13).

Monitor	Layer 1	Layer 2	Layer 3	Layer 4	Layer 5	Layer 6
IP-1	4	4	2	1	2	8
IP-2	4	5	4	1	0	4
IP-3	4	2	4	1	4	9
IP-4	3	2	4	3	3	7

3.2 Cross-Plate Monitors During Assembly

The cross plate monitors were used to measure the gravitational sag of the cross plates supported on the sphere towers with increasing number of tube layers glued to the spacer in order compensate it with the force compensation system of the assembly setup (see [1]). The cross plate sags measured with the cross plate monitors before and after sag compensation (see [1]) are shown in Figure 12.

For the RASNIK monitor on the middle cross-plate space was only available during the assembly of the first multilayer. For the assembly of the second multilayer, the sag of the middle cross plate was reconstructed from the data of the two outer cross plate monitors and of the four in-plane monitors. This method was tested with the spacer before the glueing of the tube layers and found to be very accurate with only $1-2$ μm error (see [1]).

During continuous monitoring of the cross plate sags while the chamber was supported on the sphere towers or on the crane small periodic instabilities of the measurements in close correlation with the temperature cycle in the climatized room were observed which are shown in Figures 15 and 16, respectively.

3.3 Sphere Monitors

For the monitoring of the y- and z-positions of the six spheres on the sphere towers two multi-point monitors were foreseen, each with a laser beam pointing along one side of the chamber and passing through transparent MPA-ALMY sensors mounted on the assembly table as reference and on the sphere holders at the ends of the cross plates (see [2] and Figure 1). The laser beam paths were protected with plastic tubes of 2 cm $\times$ 2 cm cross section.

When the laser beam sphere monitors were operated in the climatized assembly room with the plastic laser beam shielding tubes, it turned out that their performance was considerably deteriorated by unexpectedly large instabilities in the pointing of the two laser beams.

The laser spot position in vertical direction (y-coordinate) on the reference sensor MP-RR2 the furthest away from the laser source (see Figure 1) is shown in Figure 17 as a function of time. Oscillations with amplitudes as large as 80 μm were observed with a period of 30 minutes perfectly correlated with the cycle of the air conditioning system and the air temperature. In horizontal (z-) direction, the oscillations of the laser beam position on the same sensor have the same period but show a smaller amplitude of 20 μm (see Figure 17).

The effect can be explained by a gradient of the air temperature and therefore of the air density and refractive index $n(y)$ transverse to the laser beam inside the shielding tubes. To produce a deflection of the light rays of $\Delta y = 80\ \mu m$ over a $L = 4$ m long path a temperature gradient of $dT/dy = 0.1°\mathrm{C/cm}$ is required according to the relation

$$\begin{aligned}\Delta y &\simeq \frac{dn}{dy}\cdot\frac{L^2}{2} \\ &= a\cdot(n_0-1)\frac{dT}{dy}\cdot\frac{L^2}{2} \simeq \frac{10^{-6}}{^\circ\mathrm{C}}\cdot\frac{dT}{dy}\cdot\frac{L^2}{2}\end{aligned}$$

where the temperature dependence of the refractive index of air is parametrized by

$$n(T) = 1 + \frac{n_0 - 1}{1 + a\cdot T[°\mathrm{C}]}$$

with $n_0 = n(T = 0°\mathrm{C}) = 1 + 3\cdot 10^{-4}$ and $a = 3.6\cdot 10^{-3}/°\mathrm{C}$.

Measurements of the temperature of the plastic tube walls confirmed that such large temperature gradients are indeed present inside the plastic shielding tubes in the climatized room. Figure 18 shows the oscillations of the measured temperature difference between top and bottom of the plastic tube with an amplitude of 0.2°C and with the period of 30 minutes of the air conditioning system. The temperature gradient inside the 2 cm $\times$ 2 cm tubes therefore varies by $\pm 0.1°$C/cm in good agreement with the expected value. In addition, the average temperature difference between top and bottom differs from zero by about $+0.2°$C. A constant vertical temperature gradient on the shielding tube can be caused by the continuous illumination of the tube from above during the measurements (in a similar way as observed for the granite table; see section 1).

The following solutions of the problem have been investigated:

1. Attempts to sufficiently insulate the shielding tubes thermally from the environment did not succeed.

2. Wrapping of the plastic tubes in aluminum foil.

   Measurements of the vertical and horizontal temperature difference between the walls of of a plastic tube with and without wrapping in the assembly room (in the heating regime of the air conditioning system) are shown in Figures 19 and 20. The amplitude of the oscillations of the temperature gradient with the cycle of the air conditioning system as well as the average temperature gradient are both reduced by an order of magnitude compared to the unwrapped plastic tube due to reflection of the ambient light and the better thermal conductivity of the tube wall. In horizontal direction, oscillations of the temperature gradient of the same magnitude as in vertical direction are measured but the average temperature gradient is zero in contrast to the vertical case.

3. Heat conducting metal shielding tubes.

   Such tubes can relatively easily be installed. The decoupling of the inside of the tubes from temperature gradients developing on the outer surface improves with increasing wall thickness (see Figure 21).

   With a round aluminum tube with 30 mm outer diameter and a wall thickness of 1 mm the temperature gradients inside the tube can be reduced such that the position variations of the laser spot at a distance of about 4 m from the source are below 2 μm in the clean room in the heating regime. Figure 21 shows the measured variations with the cycle of the air conditioning system. The laser beam stability achieved with the "thick" aluminum tube is sufficient for the laser sphere monitoring system.

   The effect of a temperature gradient constant in time, e.g. due to illumination of the shielding tube from above was not measured. If it exists for the "thick" aluminum tube, it can be reduced with better reflectivity of the tube outer wall.

   Without shielding tube, the laser beam deflections in vertical direction are significant. Figure 21 also shows that plastic shielding tubes stronly enhance the effect of tenperature gradients in the air on the laser beam.

4. Increased local air flow in the room transverse to the shielding tubes (using fans) in order to smoothen temperature gradients on the surface of the tubes.

5. Longitudinal air flow through the shielding tubes to smoothen temperature gradients inside.

   The effect on the laser beam stability is rather sensitive to the magnitude of the air flow. If it is too low, there is no improvement. If it is too high, turbulance, especially at the tube ends, can even increase deflections of the laser beam. Therefore and because of the extra effort needed, this method will not used.

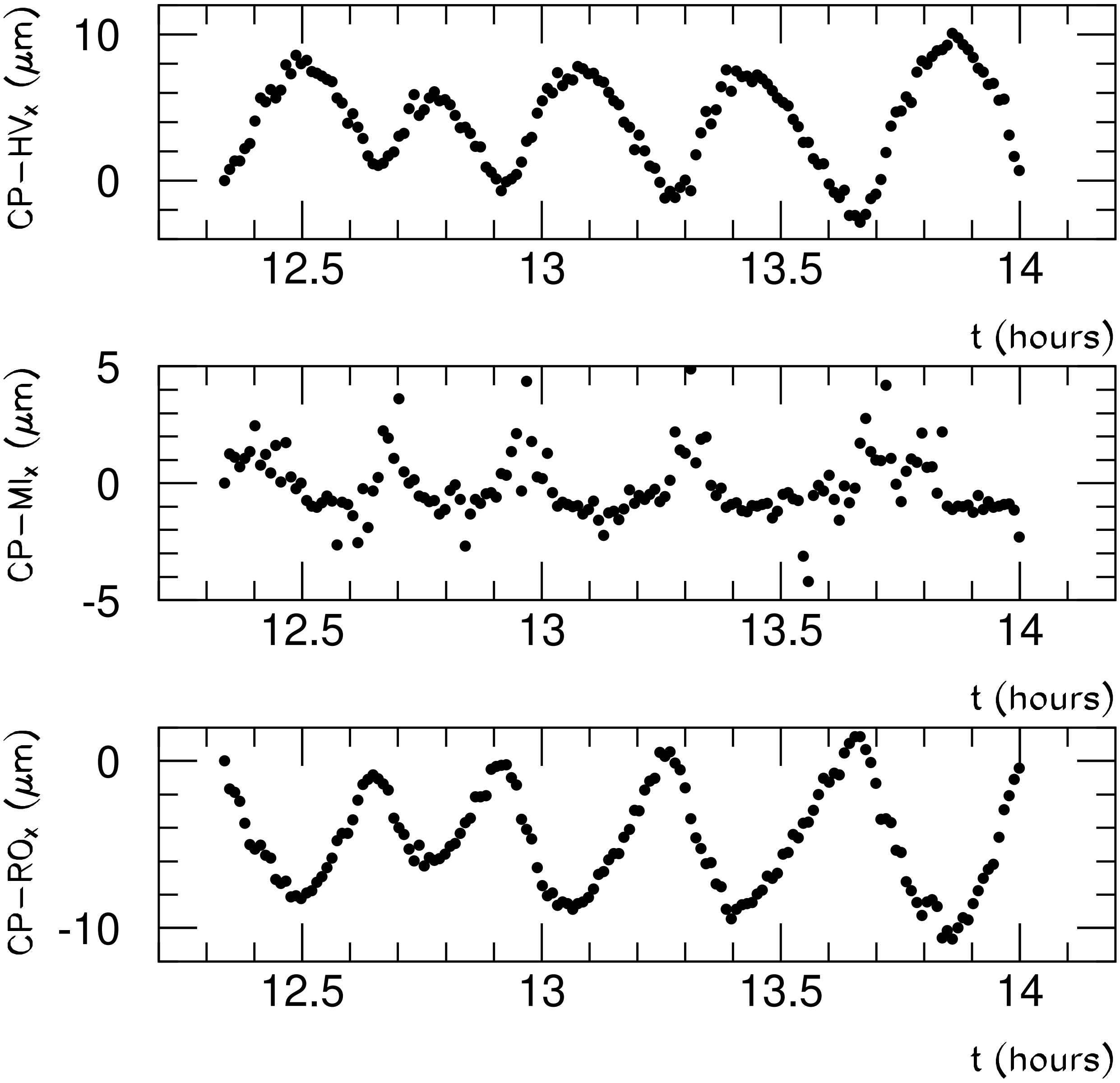

Fig. 11: Variation with time of the bending of the three cross plates in x-direction before glueing of the tube layers

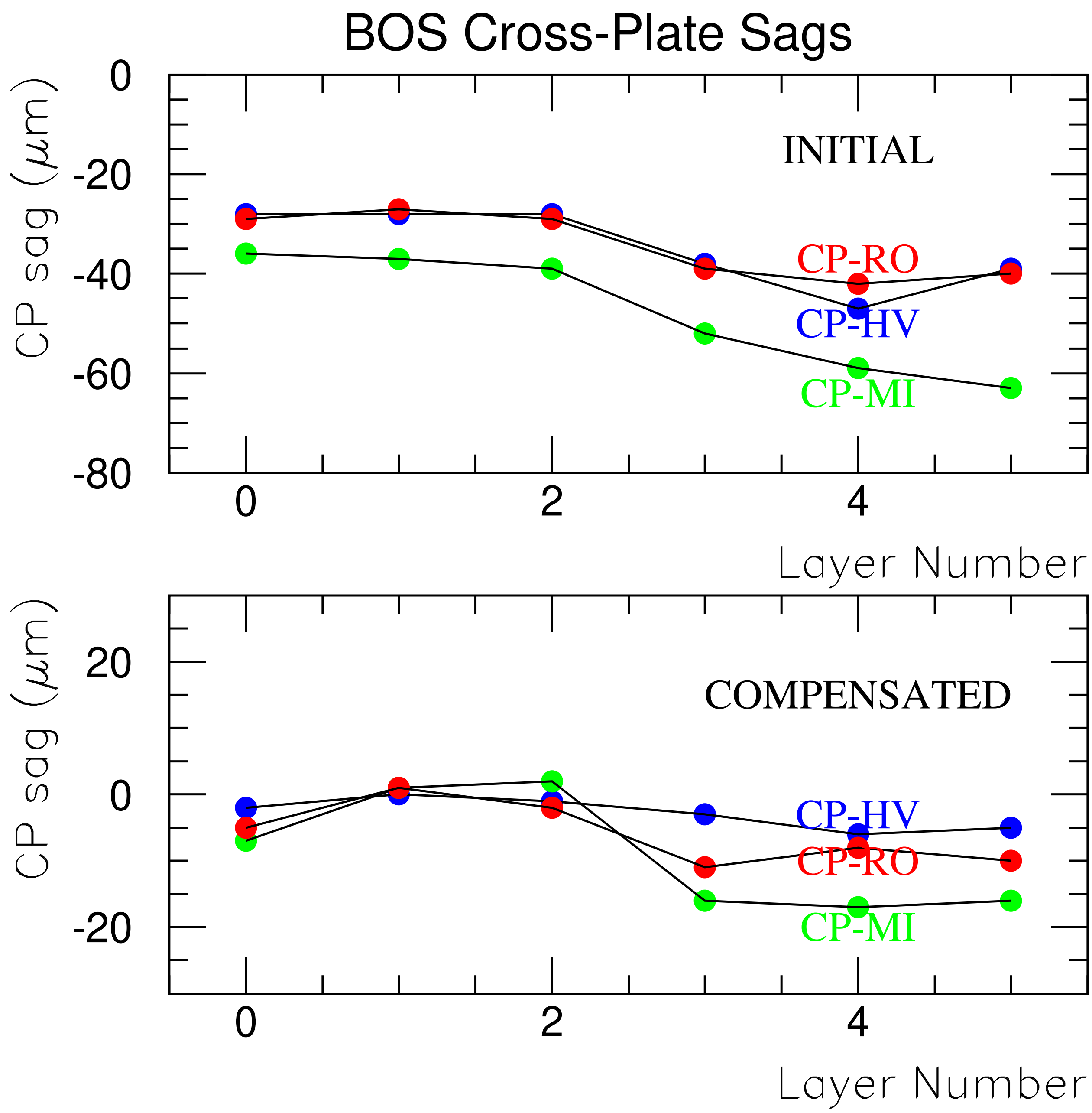

Fig. 12: Sag of the cross plates on the high voltage (HV) and readout (RO) side and of the middle (MI) cross plate before and after sag compensation during glueing of the tube layers 1–6 as measured with the cross plate RASNIK monitors (the y-axis is always pointing upwards)

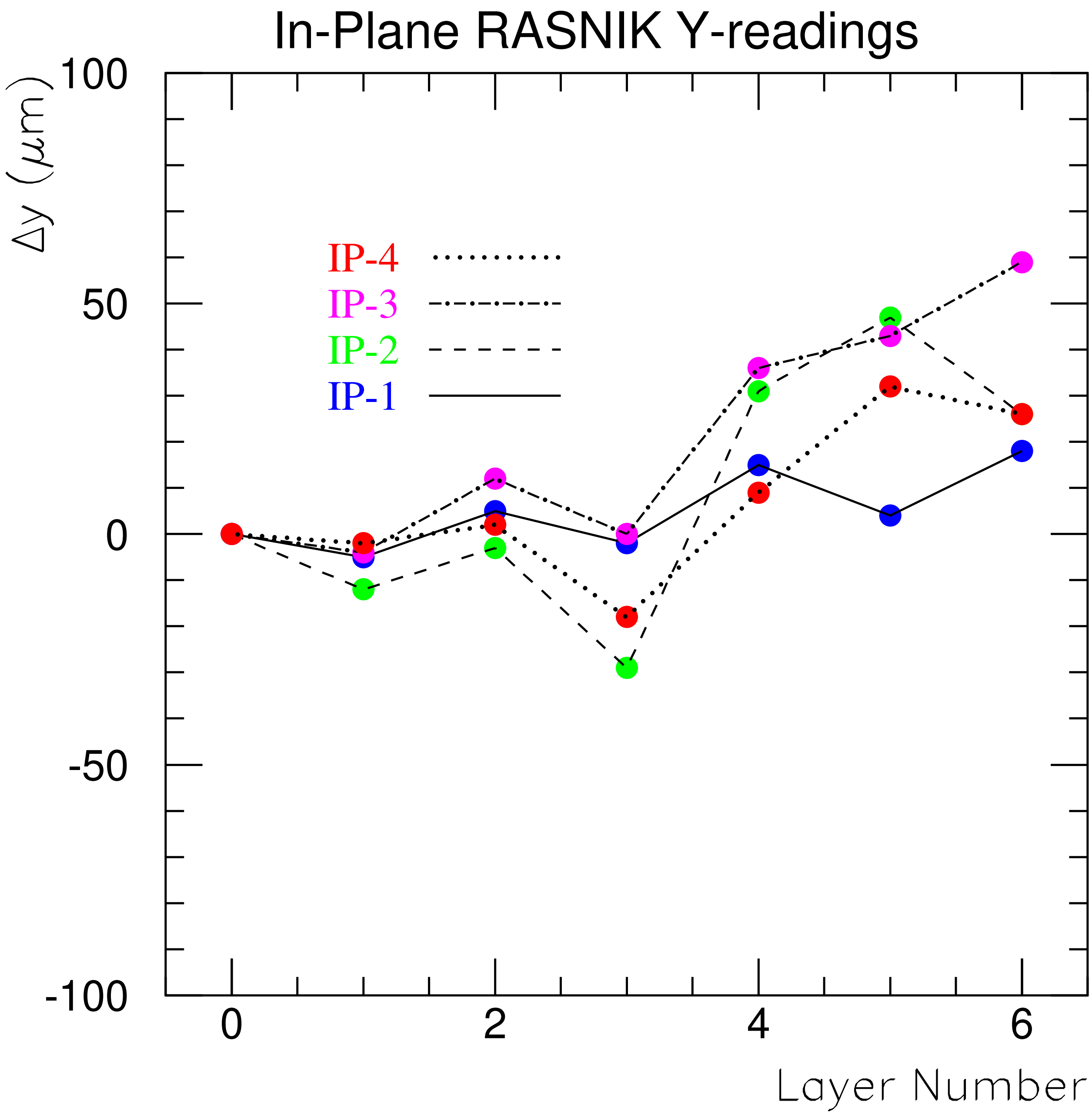

Fig. 13: Stability of the y-readings of the in-plane RASNIK monitors IP-1...IP-4 during assembly of the chamber (glueing of six tube layers) relative to the zero-readings taken with the spacer alone. The corresponding relative displacements of the middle cross plate are a factor 1/2 smaller than the readings shown (in the chamber coordinate system for the initial (INI) orientation).

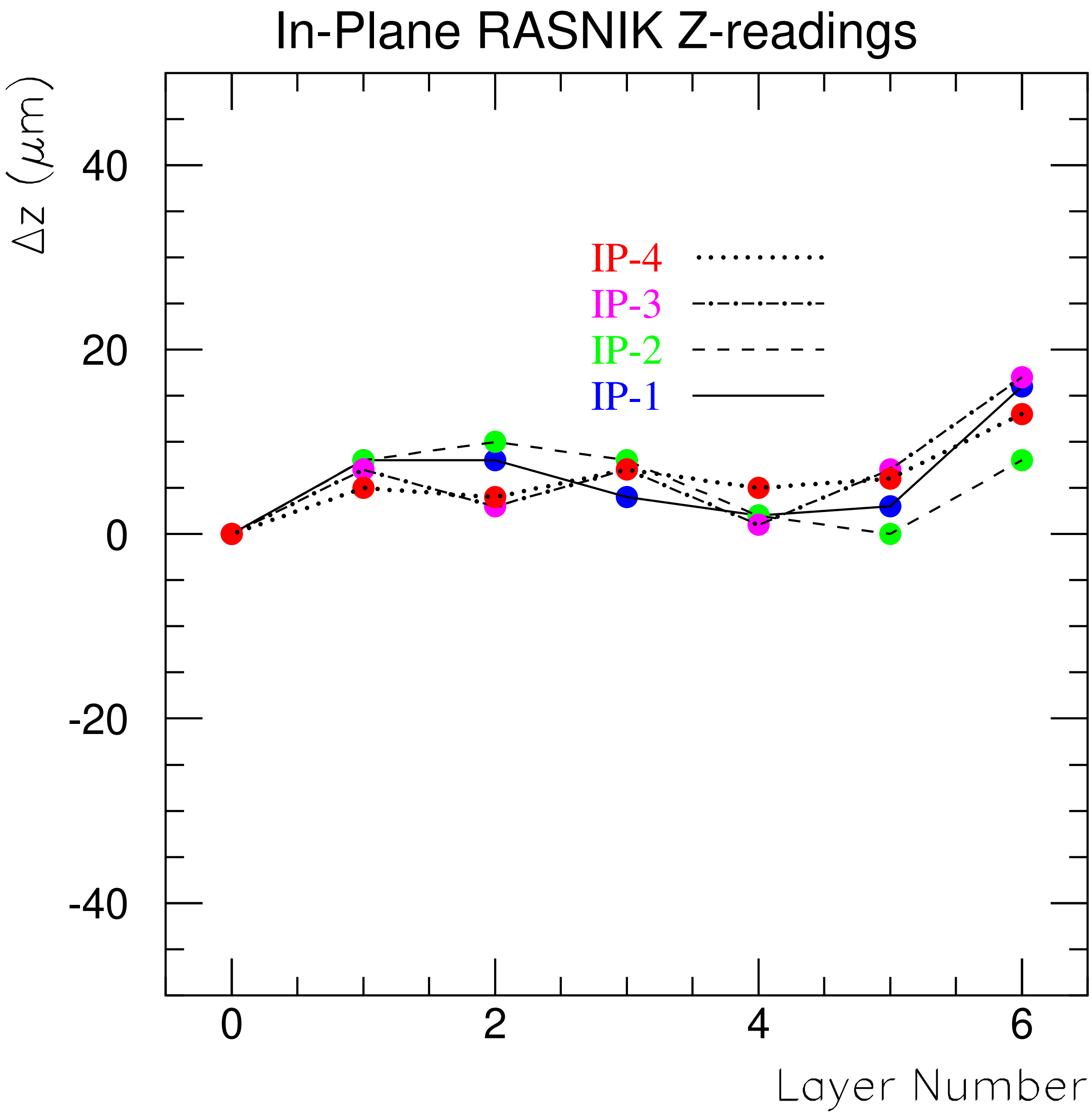

Fig. 14: Stability of the z-readings of the in-plane RASNIK monitors IP-1...IP-4 during assembly of the chamber (glueing of six tube layers) relative to the zero-readings taken with the spacer alone. The corresponding relative displacements of the middle cross plate are a factor 1/2 smaller than the readings shown (in the chamber coordinate system for the initial (INI) orientation).

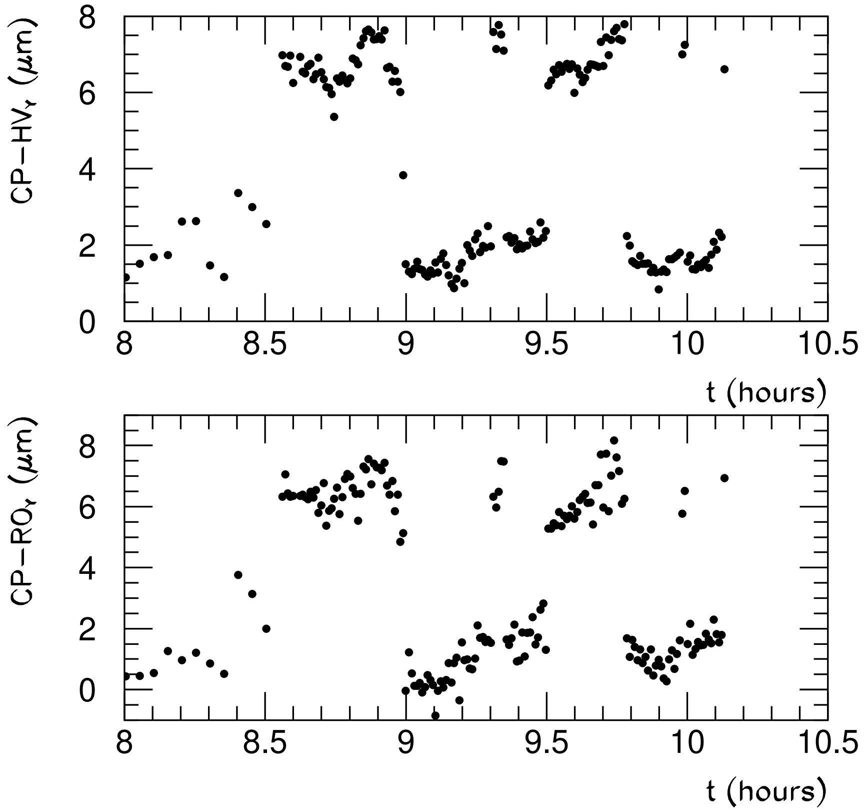

Fig. 15: Variation with time of the y-sag of the two outer cross-plates after glueing of the 4$^{\text{th}}$ tube layer while the chamber is still on the jigs and the vacuum of the combs is on

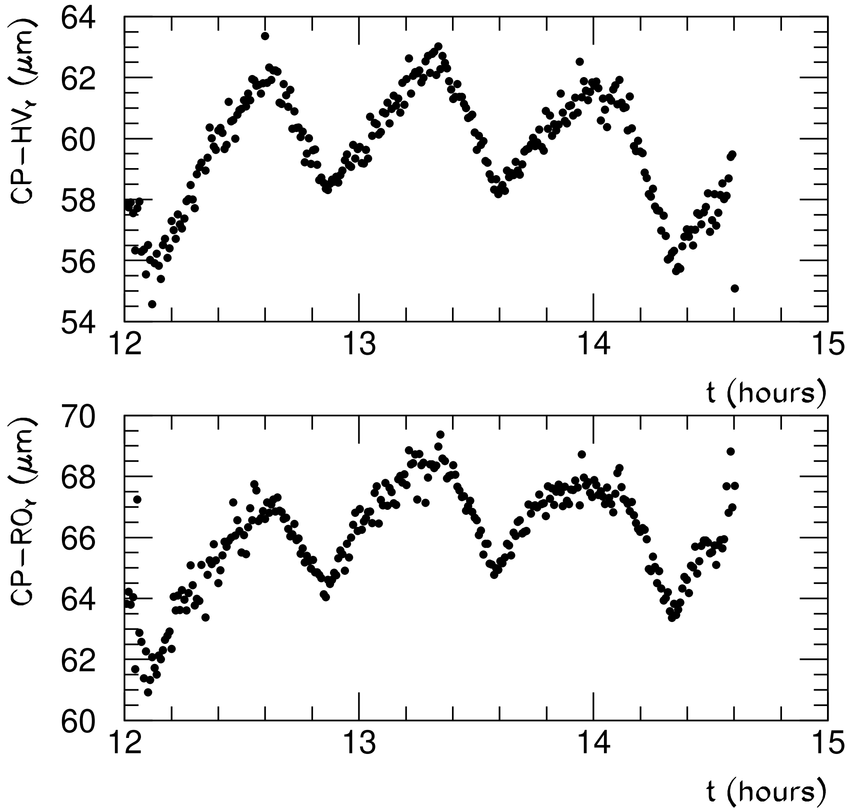

Fig. 16: Variation with time of the y-sag of the two outer cross-plates after glueing of the 5$^{\text{th}}$ tube layer while the chamber is supported horizontally on the crane

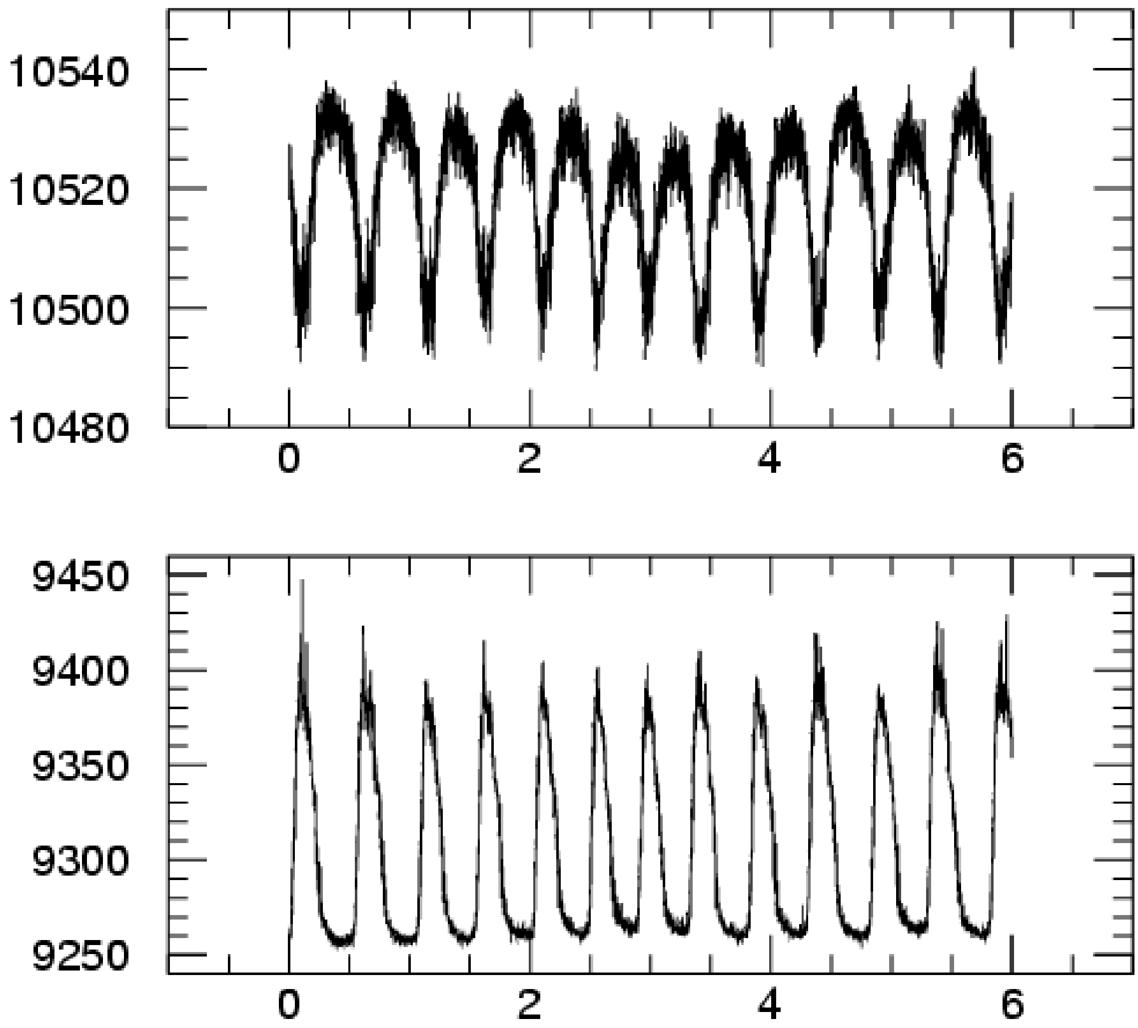

Fig. 17: Variations of the laser beam position measured on a reference sensor of the sphere monitoring system on the assembly table at a distance of about 4 m from the laser collimator as a function of time [hours]: z-coordinate [mm] (top) and y-coordinate [mm] (bottom) with arbitrary offsets

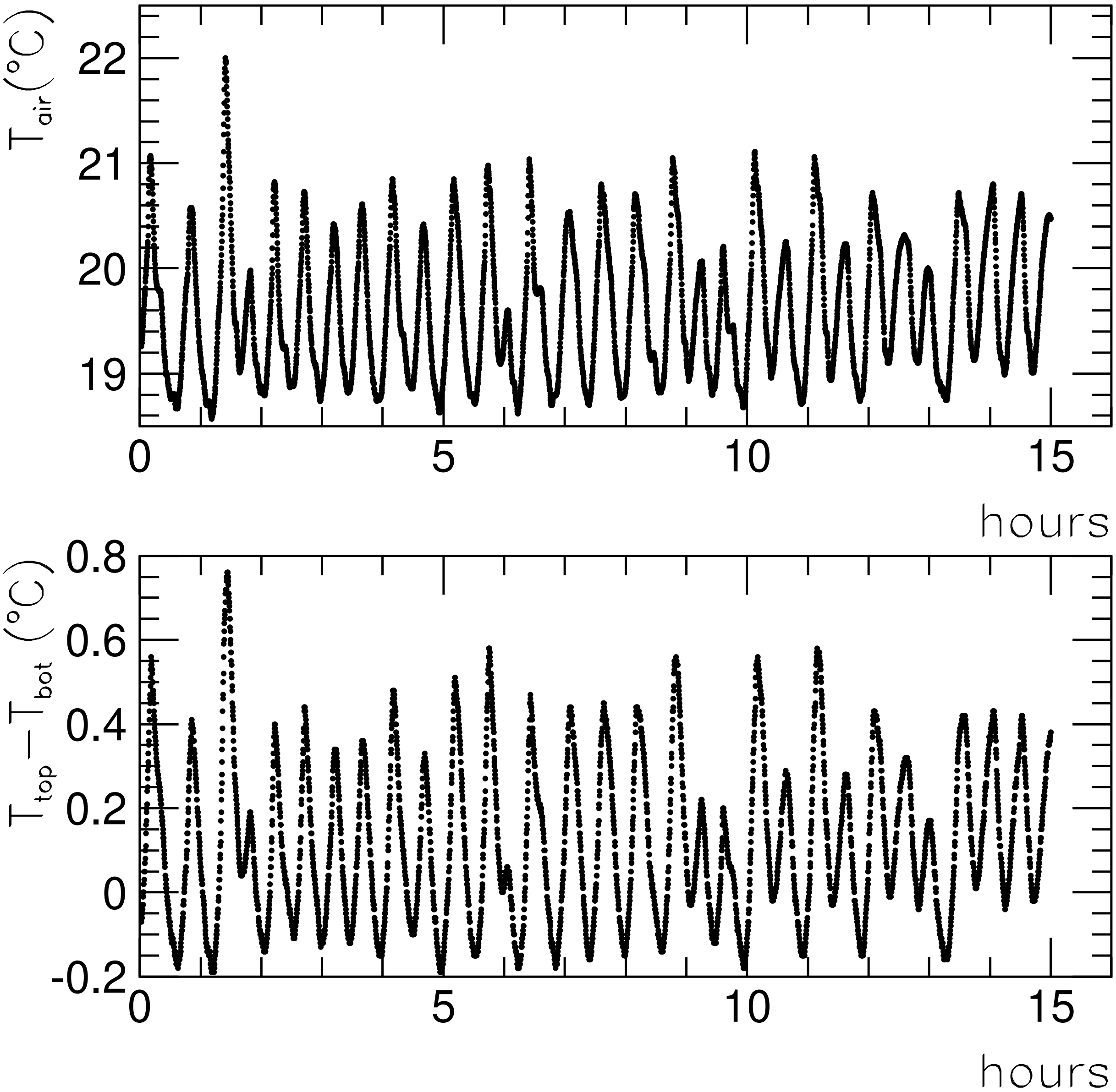

Fig. 18: Correlation between the variations of the air temperature in the climatized assembly room and of the vertical temperature difference between top and bottom of the plastic laser beam shielding tube (2 cm diameter)

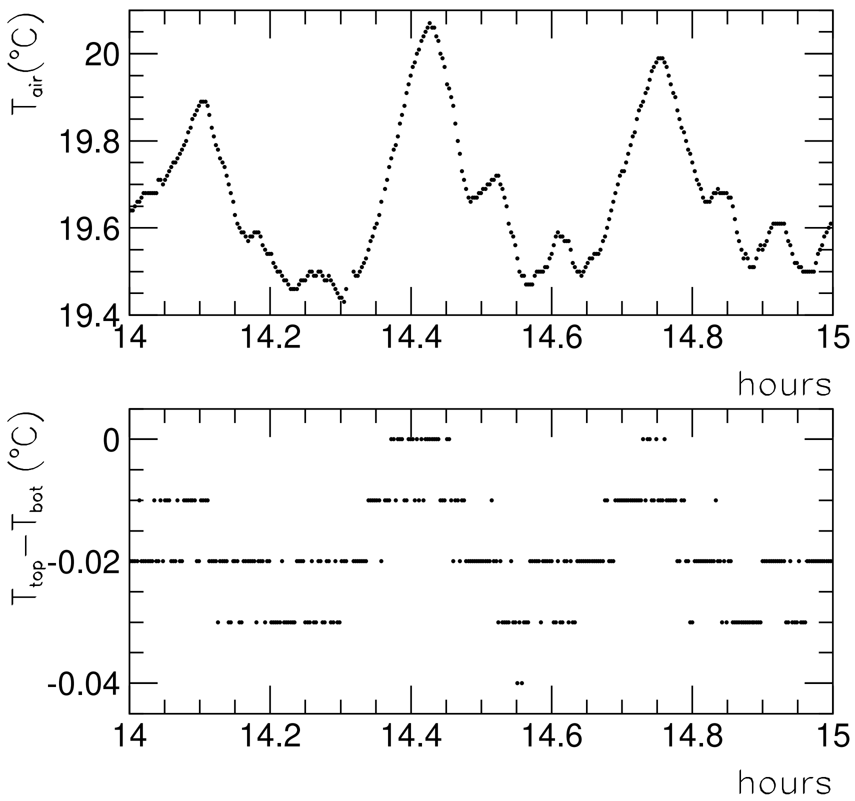

Fig. 19: Correlation between the variations of the air temperature and of the vertical temperature difference between top and bottom of the plastic tube wrapped in aluminum foil

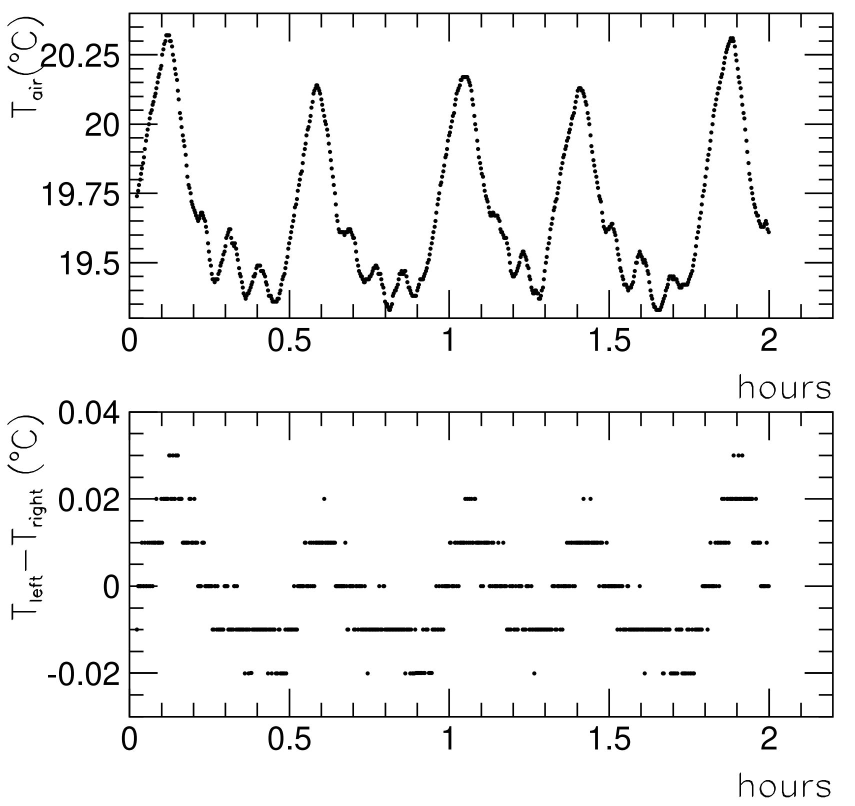

Fig. 20: Correlation between the variations of the air temperature and of the horizontal temperature difference between the walls of the plastic tube wrapped in aluminum foil

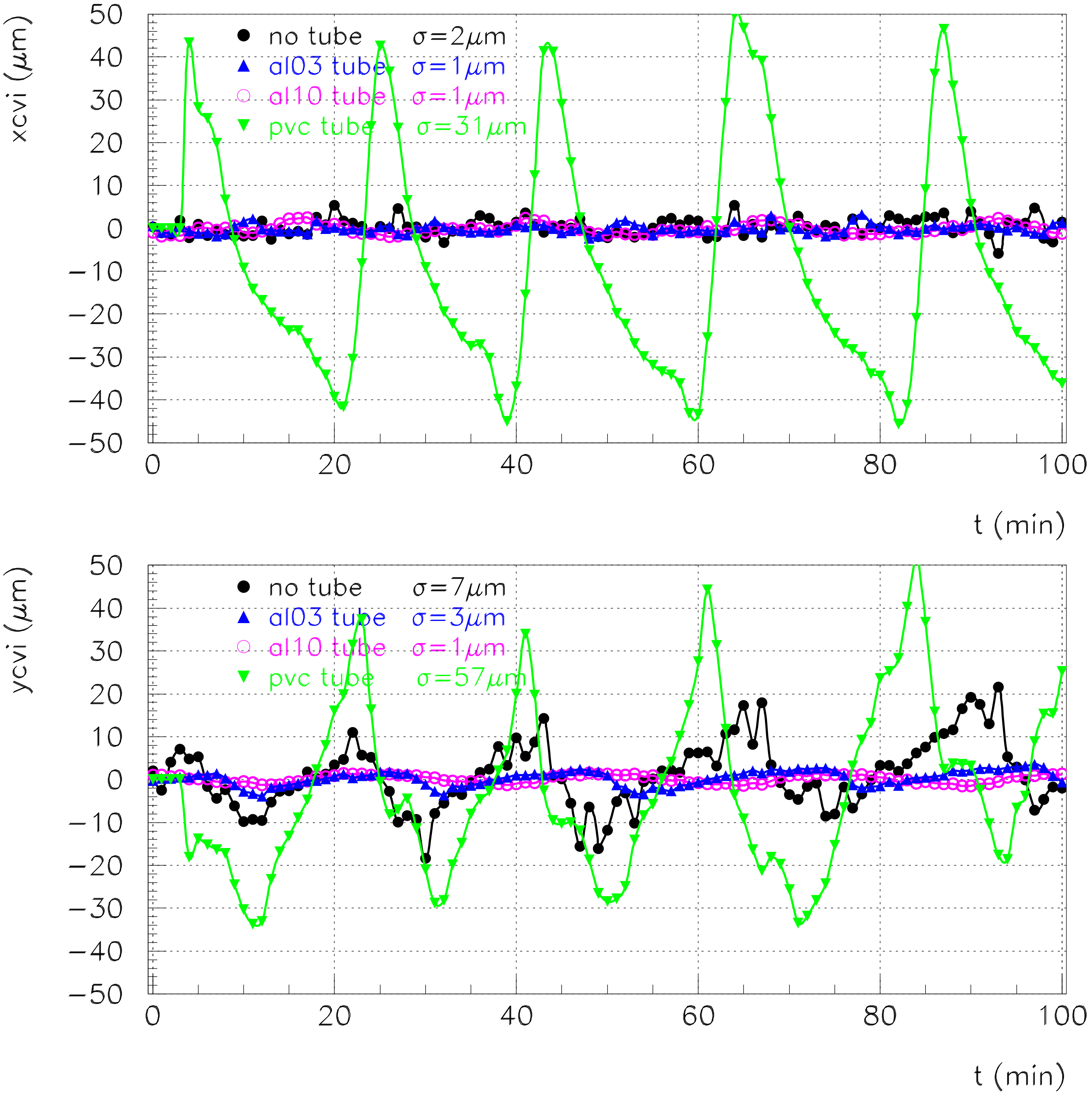

Fig. 21: Variations of the laser spot position with time at a distance of about 4 m from the laser collimator on the granite table in the assembly room with different beam shielding tubes (MDT tubes have a wall thickness of 400 μm). The periodic variations follow the cycle of the air conditioning system in the heating regime.

4 Conclusions

The detailed analysis of the optical monitoring data taken during the construction of the BOS 98 prototype chamber shows their importance for the control of the assembly process. The data have been used to optimize the assembly procedure. The influence of the thermal environment in the assembly room on the chamber and on the optical monitors (laser beams) has been studied and understood in detail. The results of the analysis give confidence in the capability of the assembly method to achieve the required mechanical accuracy of the chambers in series production.

References

[1] V. Bartheld et al., *Construction of the Full-Scale Prototype of a BOS MDT Chamber*, ATL-MUON-98-256, October 1998.

[2] H. Kroha and S. Schael, *Optical Monitoring System for the MDT Assembly Stations*, ATL-MUON-97-156, April 1997.

[3] *ATLAS Muon Spectrometer–Technical Design Report*, CERN/LHCC/97-22, ATLAS TDR 10, 31 May 1997.

[4] H. Kroha, A. Manz and A. Ostapchuk, *Analysis of the X-Ray Tomograph Data of the BOS MDT Prototype Chamber*, ATL-COM-MUON-99-025, August 1999.

[5] H. Kroha, *Quality Assurance and Control Reference Document for ATLAS MDT Chamber Construction*, ATL-COM-MUON-99-026, May 1999.